

Enabling phase stabilization of quantum networks via displacement-enhanced photon counting

M. V. JABIR,^{1,*}  D. AHN,^{1,2} N. FAJAR R. ANNAFIANTO,¹ I. A. BURENKOV,^{1,2}  A. BATTOU,¹ AND S. V. POLYAKOV^{1,3}

¹National Institute of Standards and Technology, Gaithersburg, Maryland 20899, USA

²Joint Quantum Institute and University of Maryland, College Park, Maryland 20742, USA

³Department of Physics, University of Maryland, College Park, Maryland 20742, USA

*jabirmv081@gmail.com

Received 5 September 2024; revised 19 February 2025; accepted 21 March 2025; published 23 April 2025

Optical phase stabilization, tracking, and locking in long fiber links are pivotal for the functionality of many communication protocols and distributed sensors. However, conventional phase stabilization methods use strong optical probe signals that may contaminate and destroy fragile quantum signals propagating in the same fiber link. Here, we experimentally demonstrate phase locking of fiber spools up to 100 km and over 120 km deployed optical communication link using faint coherent states with an average of just $\approx 650,000$ photons per second detected at the receiving detector as a probe signal. The power spectral density of phase noise, integrated from 1 Hz to 50 kHz, yields an excess rms phase noise of 110 mrad (corresponding to timing jitter below 0.09 fs) for a 100 km fiber spool and 140 mrad (corresponding to rms timing jitter below 0.12 fs) for deployed fiber. The displacement-enhanced measurement protocol that we employ for phase stabilization yields Fisher information that is greater than that of homodyne and heterodyne measurement protocols for fiber links longer than 100 m and, therefore, exceeds the canonical shot noise limit of accuracy. By implementing this stabilization strategy with a 50% duty cycle, we enable time-division multiplexed faint light and quantum payloads to coexist within the same communication channel. © 2025 Optica Publishing Group under the terms of the Optica

Open Access Publishing Agreement

<https://doi.org/10.1364/OPTICA.540759>

1. INTRODUCTION

Faint light [1] is increasingly used in optical networks and distributed sensors. Most notably, actively developing quantum networks require single photons, squeezed light, and other exotic states for exchanging quantum bits and distributing the entanglement [2–6]. Maintaining a known optical phase between nodes is essential for many quantum network protocols, such as entanglement swapping, quantum-repeaters-enabled long-distance communication, and optical interferometry in telescope arrays assisted by quantum networks [7–11]. A faint coherent state paired with quantum state discrimination can be used for resource-efficient classical communication, enabling the multiplexing of quantum and classical traffic in the same network, but those protocols are typically phase-sensitive [12–14]. Additionally, distributed optical fiber sensors often require phase measurement and correction for accurate and reliable operation [15,16]. While optical fibers are a convenient medium, environmental factors such as acoustic noise and temperature fluctuations result in a significant phase variation of fiber links over time. This problem is known in classical networks, and multiple solutions exist to either extract or cancel phase instability effects [17–20]. Typically, to extract a phase reference, strong classical light is used as a probe signal [21–23]. However, strong probe signals introduce broadband noise into

faint quantum channels via, e.g., Raman scattering [24–26], preventing the scalable use of wave-division multiplexing. The level of noise can be decreased by spectral detuning of quantum and classical channels, but phase references in spectrally detuned channels do not directly correspond to these in the target channel [27]. Alternatively, noise can be controlled by time-division multiplexing (TDM) of the quantum payload and the strong probe signal [28–30]. Unfortunately, to be effective, long dark time bins are necessary to prevent cross-talk due to Rayleigh and in-band Brillouin scattering and multiple back-reflections at the fiber interfaces. Indeed, the dark time bin should be equal to the round-trip time of the optical signal through the network link. Such a lengthy dark time bin will limit the stabilization bandwidth beyond that required for the phase noise cancellation in links longer than a few kilometers. Therefore, strict power limitations for coexisting probe signals must be applied to preserve quantum information.

We will refer to states of light that are weak enough so that they can be detected by single-photon detectors without significant saturation as faint light [1]. Recently, phase estimation [31,32] and stabilization [33–36] with faint coherent light were demonstrated in short fiber links (low-frequency noise regime), but proposed methods were not demonstrated in and may have limited applicability for longer links with higher-frequency noise. In this work, we use faint coherent states as a probe signal with a duty factor of

50% to allow TDM of user quantum payloads. Our phase stabilization technique uses photon-counting detectors, common in quantum networks, and employs a displacement-enabled phase estimation protocol that yields Fisher information (FI) above the homodyne and heterodyne limits [31]. We use probe signal pulses with an average of 650,000 photons per second for phase tracking and stabilization. This optical power is more than 4 orders of magnitude lower than that of conventional phase stabilization techniques that use strong optical reference pulses, e.g., with optical powers as high as a few nanowatts for the stabilization of over 100 km long common fiber links [37].

We offer a systematic study of the phase noise accumulated in fiber links of different lengths up to 100 km with interferometric visibility of above 88% using faint light stabilization. We have also successfully stabilized the phase of the deployed fiber loop spanning over 120 km between the National Institute of Standards and Technology (NIST, Gaithersburg campus) and the University of Maryland (UMD, College Park campus) with interferometric visibility of above 86%, sufficient to demonstrate quantum effects [38,39].

To our knowledge, this is the first report on optical phase tracking and stabilization for metropolitan-scale optical networks that employs a faint probe signal and photon-counting-enhanced phase sensing. This work enables the scalable use of metropolitan-scale optical fiber networks for multiplexed and coexisting classical–quantum traffic. It also enables essential quantum networking protocols, including DLCZ-like [40] quantum repeaters for intercity entanglement distribution.

2. EXPERIMENT

Using faint coherent light as probe signals for phase tracking and stabilization requires the application of single-photon detectors and enables measurement methods from the quantum playbook. In particular, because the quantum resource in the probe states is limited, it is important to maximize the quality of the estimator, if possible, beyond the conventional measurement means. To this end, it was shown that the quantum Fisher information (QFI) of the phase estimator for coherent states is a constant that does not depend on the measured phase and is greater or equal to the FI offered by either a homodyne or a heterodyne arrangement. While a measurement at the QFI limit may be hard, displaced photon counting provides the FI advantage over homodyne and heterodyne methods in the wide vicinity of a certain (target) phase.

This phase estimation scheme is inspired by quantum receivers [14] and has been introduced by Izumi *et al.* [31]. The displacement-based photon-counting measurement is described by a displacement operator $\hat{D}(\beta)$, where $|\beta\rangle$ represents the coherent state of the reference light. This operator is applied to the coherent state of the probe signal at a beam splitter, as shown in the bottom inset of Fig. 1. Note that the transmittance/reflectance ratio of the displacing beam splitter is arranged such that 99% of the probe signal and 1% of the reference light impinge on the detector to improve overall system efficiency. When applied to the probe coherent state $|\alpha\rangle$, we require that $\hat{D}(\beta)|\alpha\rangle = |\text{vac}\rangle$, where $|\text{vac}\rangle$ is the vacuum state when the phase of $|\alpha\rangle$ is equal to that of the target. The advantage occurs because displacement measurements are set to displace the probe faint coherent state to vacuum with subsequent verification by a single-photon detector. In our work, we use displacement measurements to implement the phase stabilization protocol for metropolitan-scale optical networks.

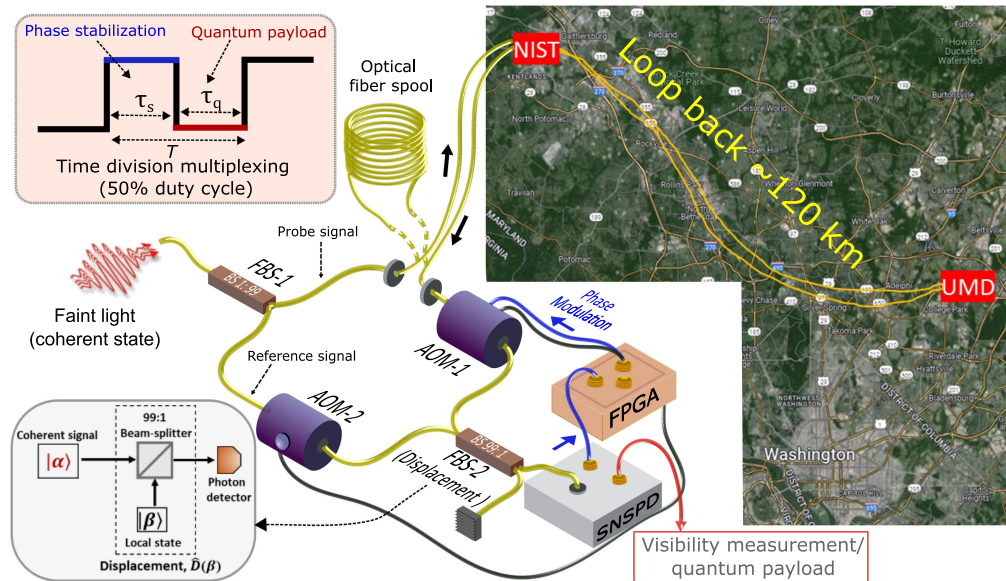


Fig. 1. Experimental setup for phase stabilization. An attenuated ultra-stable reference laser is sent through a 1:99 fiber beam splitter 1 (FBS-1) into an unbalanced Mach–Zehnder interferometer. One arm of the interferometer carries the probe signal through a long optical fiber spool or a deployed fiber loop, while the other arm uses a short fiber to carry the reference light. Acoustic optical modulators (AOMs) are used to modulate phase and frequency in both arms. The optical probe signal from the long arm is displaced by the reference light in the short arm at the 99:1 FBS-2 and detected by a superconducting nanowire single-photon detector (SNSPD). Photon detection events are analyzed with a field programmable gate array (FPGA), which estimates the phase drift in the fiber link. Then the FPGA applies a compensating phase shift to the input fiber link (long arm, ACM-1) to match the phase of the displacement signal in the short arm and achieve destructive interference at the interferometer output (i.e., the displacement to vacuum). Inset in the bottom left: the displacement-based photon-counting protocol; see text. Inset in the top left: time-division multiplexing used in this work. The phase stabilization signal operates with a 50% duty cycle to accommodate quantum or classical, but faint payloads. Imagery © 2024 TerraMetrics. Map data © 2024 Google.

The aim of phase tracking and stabilization is to ensure that the phase of the input probe signal is continuously known with high accuracy. Here, a feedback mechanism compensates small phase deviations of the input probe signal with respect to the reference signal in order to maintain the phase lock, i.e., the phase difference measured by this method is nearly always small. Thus, by design, our tracking protocol overcomes the shot noise limit that bounds the performance of the homodyne and heterodyne measurements. We systematically estimate the degree of advantage obtained with this method using Fisher information.

The experimental setup is shown in Fig. 1. We utilize a faint signal in the C-band (1550 nm) from the ultra-stable laser to stabilize the long optical fiber link with displacement measurement and single-photon detection. The ultra-stable laser boasts a spectral width of just a few Hz, resulting in a coherence length of thousands of kilometers and negligible phase noise. For this demonstration, we use an unbalanced Mach–Zehnder interferometer (MZI) to extract the phase information and phase lock the fiber link. The laser light is split using a 1:99 fiber beam splitter (FBS-1), and 1% output is sent through the long fiber (optical fiber spools and deployed fiber), which serves as a probe signal, while 99% is sent through the short fiber with 1 m length and serves as a displacing reference signal $|\beta\rangle$ (local oscillator). Subsequently, the displacement occurs at FBS-2, where the coupling ratio is 99:1, meaning that 99% of the signal from the probe (long) arm is transmitted, while 1% of signal from the reference (short) arm is reflected. The intensities at the output of FBS-2 are balanced by adjusting the intensity of the reference signal to match that of the probe, leading to destructive interference (displacement to vacuum), thereby achieving maximal interferometric visibility. The splitting ratio of the first beam splitter (FBS-1) is not relevant to the protocol, so long as light is balanced on the FBS-2. We use acousto-optical modulators (AOM-1 and AOM-2) to frequency-modulate both channels, and the AOM-1 is also used to compensate for phase noise introduced by the fiber spool. Alternatively, for phase-tracking applications, AOM-1 can be placed before the long fiber link, and AOM-2 can be used to adjust the phase of the local oscillator and track the phase of the input, which would reduce the power of probing states that traverse the fiber even more.

The output of the FBS-2 is connected to a commercial superconducting nanowire single-photon detector (SNSPD) with an estimated detection efficiency of 95.7(5)%, a recovery time of around 30 ns, a timing jitter of < 100 ps, and a dark count rate of $\nu \approx 10$ counts/s. The SNSPD photoelectronic detection pulses are sent to the FPGA for photon counting, phase shift estimation, and feedback control (see Section 1 of Supplement 1 for details). Since the goal of this work is to develop a phase-stabilized optical fiber link for blended networks with coexisting classical–quantum traffic, we implement time-division multiplexing to send the probe signal for τ_s , with τ_q reserved for the quantum or classical faint payload, as shown in the upper left inset of Fig. 1. The duty factor τ_q/T in our experiment is 50%, but it can be arbitrary so long as τ_s is significantly longer than the detector's recovery time and $T = \tau_s + \tau_q$ is shorter than the phase fluctuation times. The cycle duration, T , is adjusted for different fiber lengths to optimize the feedback bandwidth, and the average number of photons per pulse that we used varies from 6.5 to 97.5 for τ_s , from 10 to 150 μ s correspondingly (see Section 1 of Supplement 1 for details). In all the experiments, we keep the detected probe power (measured as the average number of detected photons during τ_s) constant at

$\approx 650,000$ photons per second, equivalent of ≈ 83 fW with 0.5% statistical uncertainty. This number is estimated by averaging the number of detections per second over 200 data points during τ_q when light from the reference path is blocked. To provide out-of-the-loop verification of phase stability, we measure the visibility of the interference fringe during the quantum payload time τ_q .

In this experiment, we use optical fiber spools ranging from 1 m to 100 km to characterize the performance of our stabilization method as a function of the fiber link. We also stabilized the deployed optical 60 km fiber link in a loopback configuration (a total of 120 km). This particular link is between the National Institute of Standards and Technology (NIST) and the University of Maryland (UMD), artistically depicted in Fig. 1 (the exact fiber layout is not disclosed). The fiber link consists of multiple SMFs interconnected through passive optical switches and fiber patch panels, not shown in the figure. Note that this fiber link is primarily aerial ($\approx 75\%$). Therefore, we anticipate increased noise and instabilities due to environmental factors such as temperature variations and wind.

Quantum or faint light payloads can be launched along with the probe signal with an extra unbalanced FBS. The single-photon detectors used for stabilization can, in principle, be reused for quantum payload detection by switching the reference signal off. However, a particular quantum protocol defines a particular way of quantum signal injection in the phase-stabilized channel.

3. RESULTS AND DISCUSSION

A. Fisher Information Advantage

The error associated with phase estimation due to the measurement uncertainty depends on the choice of a measurement strategy and follows from the Fisher information calculations. It is well understood that, for an unbiased estimator, the ultimate lower bound for variance is given by the Cramer–Rao bound, $\text{Var}[\phi] \geq 1/(M \times QF(\phi))$, where M is the number of measurements and $QF(\phi)$ is the quantum Fisher information [41]. In the ideal case, the QFI for the phase measurement with coherent states does not depend on the phase ϕ and is given by $QF(\phi) = 4\langle n \rangle$, where $\langle n \rangle$ is the average number of photons. When classical phase measurements such as homodyne and heterodyne detection are used, the FI for a given average photon number is $F_{\text{hom}}(\phi) = 4\langle n \rangle \cos^2[\phi]$ and $F_{\text{het}}(\phi) = 2\langle n \rangle$, respectively. It can be shown that displaced photon counting yields better FI than either homodyne or heterodyne measurements for a wide range of phases [31]. The FI for ideal displacement photon counting is $F_{\text{dis}}^{\text{ideal}} = 2\langle n \rangle(1 + \cos[\phi])$. This strategy has a significant practical advantage for the measurement of phases in a relevant range of values [see Fig. 2(a)]. Displacement measurements are set to displace the coherent state to vacuum and overcome the shot noise limit that bounds the performance of the homodyne and heterodyne measurements. The shot noise limit is a specific manifestation of the standard quantum limit related to the quantum nature of light. We point out that overcoming this limit is considered a quantum advantage in the literature [42–45]. Here, we refer to this advantage as the Fisher information advantage (FA) obtained with displacement measurement compared to all canonical phase measurement arrangements (homodyne and heterodyne).

To analyze the practical performance of displaced measurement versus canonical measurements, we calculate the FI normalized

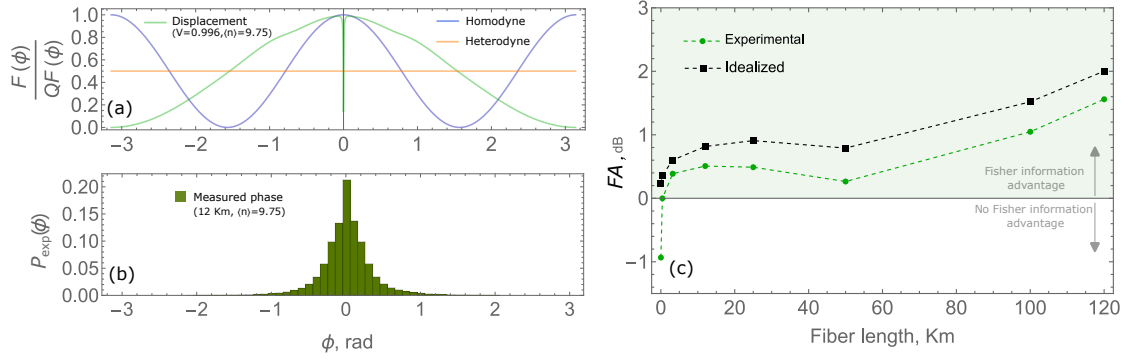


Fig. 2. (a) Comparison of Fisher information of non-ideal displacement measurement in our experiment (green curve) with classical homodyne (blue wave) and heterodyne (orange line) measurements; (b) the histogram of the phase noise measured by the phase stabilization algorithm in a 12 km optical fiber spool over 7.5 s (500,000 measurement pulses of $T = 30 \mu\text{s}$ duration with 50% duty cycle); and (c) average Fisher information advantage (FA) of displacement phase noise measurements used for the phase locking for the ideal displacement measurement (black squares) and for our experimental setup (green circles). Dashed lines are guides for the eye.

by the QFI, $F(\phi)/QF(\phi)$, considering our experimental conditions where the displacement visibility (which is also equal to the maximum achievable interference visibility, i.e., when the probe state exactly matches the reference state) is $V_D = 0.99599(1)$, and the dark count rate is $\nu \approx 10$ counts per second, as shown in Fig. 2(a). The green line illustrates the FI for our experimental case. The dip in FI at $\phi = 0$ is caused by the imperfect visibility and dark counts. As the average number of photons $\langle n \rangle$ used for the phase estimation increases, the impact of the feature reduces (see Section 2 of Supplement 1 for details). Unless stated otherwise, all reported uncertainties are statistical uncertainties; the sample size is chosen using the Allan deviation long-term stability analysis, as described later in the paper. To estimate the average effective Fisher information advantage (FA) in phase measurements, we calculate the FI of the displacement measurement for our experimental conditions $F_{\text{dis}}(\phi)$ and separately compute the histogram of the phases measured by the stabilization algorithm, $P_{\text{exp}}(\phi)$, for every given fiber length. The average Fisher information advantage of our protocol in a phase measurement is

$$FA = \frac{\int_{-\pi}^{\pi} F_{\text{dis}}(\phi) P_{\text{exp}}(\phi) d\phi}{\int_{-\pi}^{\pi} F_{\text{hom}}(\phi) P_{\text{exp}}(\phi) d\phi}, \quad (1)$$

where $F_{\text{hom}}(\phi)$ is the FI achievable in the ideal homodyne measurement. Here, we compare our method to the homodyne because its FI is maximal (reaches QFI) for the target phase. Most of the phases measured during locking fall into a sufficiently narrow range [Fig. 2(b)]. Here, we calculated the FI per detected photon without adjusting for the detection efficiency. This approach was chosen because it appropriately gauges the advantage gained by changing the detection scheme only, as opposed to employing a detector with higher (or lower) detection efficiency. We also point out that, in a comparable homodyne measurement, either a similar single-photon detector (with a similar detection efficiency) or an InGaAs photodiode (whose detection efficiency is typically significantly lower than what was used here) would be used.

We estimate $P_{\text{exp}}(\phi)$ for all fiber lengths, including the deployed link (see Section 4 of Supplement 1 for data). Then we compute FA for the ideal ($V_D = 1$, $\nu = 0$) displacement case and for our experimental conditions [see Fig. 2(c)]. As expected, the idealized displacement offers a FI advantage over the classical

phase measurement in all cases. Interestingly, displacement measurement under our imperfect experimental conditions has a clear advantage for all fiber lengths except the shortest 1 m fiber link.

B. Interferometric Visibility

To verify the quality of the phase stabilization, we use time-division multiplexing to send a probe signal instead of the quantum payload and measure the interferometric visibility. Indeed, in a perfectly stabilized link, this out-of-the-loop verification measurement should yield the vacuum state and the unit visibility. We analyze the interference pattern of the coherent signal after FBS-2 with SNSPD (see Section 3 of Supplement 1 for details). The visibility can be calculated as $V = (\langle n \rangle_{\text{max}} - \langle n \rangle_{\text{min}}) / (\langle n \rangle_{\text{max}} + \langle n \rangle_{\text{min}})$, where $\langle n \rangle_{\text{max}}$ is the maximum average photon count rate, which is about 4 times greater than the photon count rate of the probe signal (i.e., $\langle n \rangle_{\text{max}} \approx 4\langle n \rangle$). The minimum average count rate, $\langle n \rangle_{\text{min}}$, is determined by averaging the number of photons detected at the output of the stabilized interferometer. Because we operate in the photon-starving regime, to avoid extra shot noise, we do not reconstruct an interference fringe for visibility characterization. We instead measure $\langle n \rangle_{\text{min}}$ and $\langle n \rangle_{\text{max}}$ separately. Note that the $\langle n \rangle_{\text{max}}$ measurement is quite accurate, and this value does not significantly fluctuate in our measurement. Therefore, by focusing on measuring the $\langle n \rangle_{\text{min}}$, we reduce the influence of the shot noise on the visibility measurement. In Fig. 3, we show that the measured interference visibility reduces for longer optical fiber spools. For all the fiber spool lengths ranging from 1 m to 100 km, we have measured visibility greater than 0.885. Given the long-term stability of those measurements, data were accumulated for an extended time, making uncertainties small, such that error bars in the figure are smaller than the data points and therefore not visible. For the deployed optical fiber, our method achieved visibility of 0.865(5), consistent with the fiber spool measurements. The larger statistical uncertainty of this measurement is due to reduced long-term stability; see Allan deviation analysis.

The obtained visibility allows for the observation of quantum phenomena in phase-stabilized networks. For instance, Ref. [39] defines the minimal visibility required to demonstrate the non-locality of a single photon that violates the Bell inequality, necessitating phase stabilization to achieve at least that visibility. We point out that in addition to phase stabilization, other

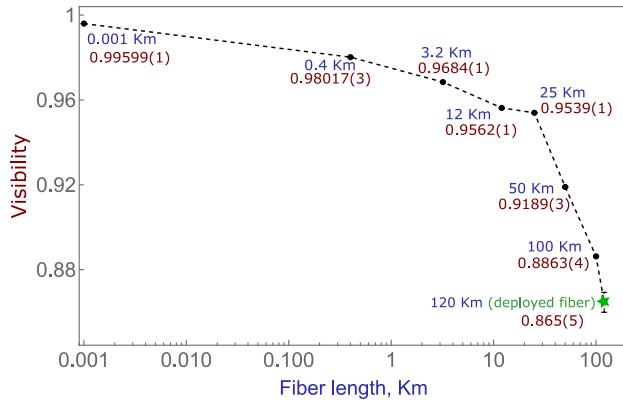


Fig. 3. Interferometric visibility achieved by stabilizing the phase of long fiber links using a faint probe signal at 1550 nm, resulting in $\approx 650,000$ photons per second detected at the receiver. The results for fiber spools of different lengths are marked with black dots, and the visibility measured in the deployed optical link is marked with a green star. The statistical uncertainty of measured visibilities is smaller than the plot markers' size for fiber spools. The dashed line is a guide for the eye.

protocol parameters should be controlled to experimentally demonstrate non-local effects; the better the phase stabilization, the less stringent these requirements are [39].

C. Phase Noise Analysis

To analyze the performance of phase stabilization in optical fiber links, we calculate the power spectral density (PSD) of the phase noise with and without the stabilization (see Fig. 4). The PSD gives a spectral characterization of the phase noise *in situ* [46]. The PSD can be calculated from the signal at the output of the unlocked interferometer; however, those measurements are limited to phases $\Phi \in (-\pi, \pi)$, and therefore discontinuities of the phase occur for the phase drift beyond 2π , resulting in apparent, but not real high-frequency noise on a Fourier transform. The unique feature of our implementation gives access to the complete record of the phases measured at each phase stabilization step from the FPGA.

We calculate the PSD of the phase noise accumulated in an unstabilized fiber link from the series of phase noise increments per each τ_s , yielding complete phase traces $\Phi \in (-\infty, \infty)$ (see Section 4 of Supplement 1 for details and data). This strategy yields the spectrum of noise undistorted by phase discontinuities.

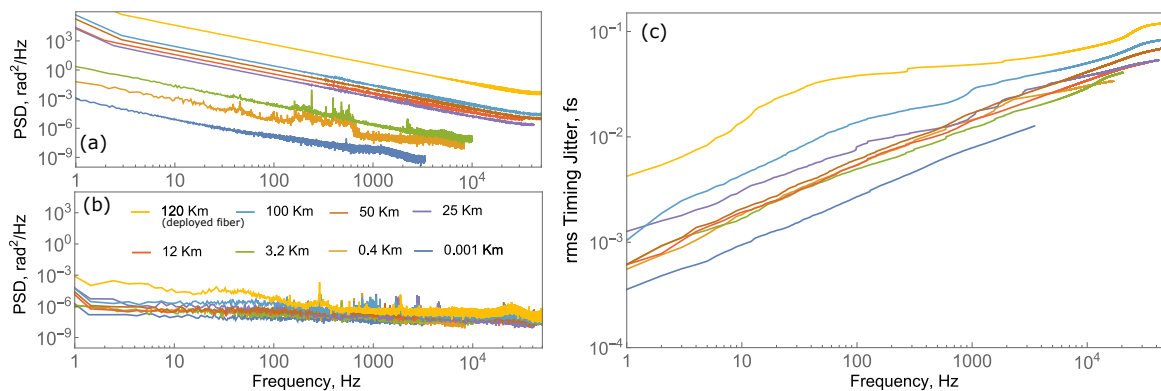


Fig. 4. Power spectral density (PSD) and timing jitter of phase noise in fiber links. (a) PSD of the phase noise recovered from the stabilization algorithm feedback (see text for details), (b) PSD of the residual phase noise obtained from the photon counting data with stabilization enabled, and (c) integrated residual phase noise displayed as rms timing jitter. Color coding corresponds to the length of the fiber link and is the same in all plots. The legend is shown in chart (b).

The bandwidths of the phase noise measurements are determined by the sampling period in the FPGA, T (refer to Table 1 in Supplement 1 for details). Since T is optimized for different fiber lengths, the resulting measurement bandwidth also differs for each length, ranging from 3.33 kHz for a 1 m fiber to 50 kHz for a deployed fiber link of 120 km. This relatively low bandwidth c.f. [33] is due to the low photon count in the probe field. Figure 4(a) shows that as the fiber spool length increases, the PSD of the phase noise with no stabilization increases.

The PSD of the residual phase noise in the stabilized fiber link is obtained from the out-of-the-loop interferometric visibility measurement. To count out-of-the-loop photons, the output from the SNSPD is routed to a time tagger synchronized with the payload part of the cycle (τ_q , shown in Fig. 1). When stabilization is enabled, we observe a significant overall reduction in the residual phase noise in all our experiments [Fig. 4(b)]. Phases are calculated from the measured count rate in the approximation of small phase fluctuations as $\phi \approx |\arccos[(1 - n_{\min}/(2\langle n \rangle)) V_D]|$, where n_{\min} are the measured photon count rates at the output of the stabilized interferometer, $\langle n \rangle$ is the average photon count rate of the probe signal, and $V_D = 0.99599(1)$ is the visibility of the displacement.

The PSD of residual phase noise is integrated from 1 Hz to the highest accessible frequency to find the timing jitter, demonstrating phase stabilization of the shortest fiber link with the timing jitter smaller than 0.01 fs and 120 km deployed fiber with 0.12 fs of jitter rms [Fig. 4(c)]. The timing jitter metric is common in the literature on frequency transfer and phase stabilization [47]. It can also be used to estimate expected error rates in quantum communication protocols. This jitter corresponds to the total accumulated rms phase noise of ≈ 10 and ≈ 140 mrad at an optical frequency of 193 THz (1550 nm), respectively.

We further analyze the long-term stability of our stabilization algorithm using the Allan deviation (ADEV) [48] (see Fig. 5). Here, we evaluate long-term variations of the interferometric visibility (phase noise). We collect visibility measurements in 1 s intervals, spanning a total duration of 2000 s for fiber spools and 200 s for the deployed fiber, and calculate the ADEV with the Stable32 software suite [49]. This key metric can be used to estimate the contribution of random, uncorrelated noise and the time scales associated with the long-term drift of the setup, e.g., due to uncontrolled fiber instabilities.

We plot the ADEV from 1 s to 500 s, where the first point in the ADEV plot shows the standard deviation of the visibility (phase

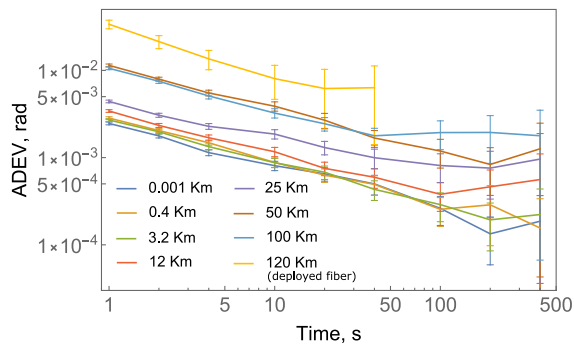


Fig. 5. Allan deviation of the phase stability for different fiber lengths.

noise) measured in 1 s intervals after stabilization is enabled, which yields an uncertainty below 20 mrad in fiber spools of up to 100 km and below 50 mrad in a 120 km deployed fiber link. For all fiber spools, the ADEV decreases for averaging times up to 200 s and is reduced to below 5 mrad. The results confirm the phase stability enabled by our phase stabilization system on a minute scale. After 200 s, the ADEV is constant or starts increasing, which may be due to the polarization drift in the fiber that may occur at the time scale of minutes. It is even more evident in the deployed fiber, where the ADEV saturates after 40 s. Due to the large polarization drift of the aerial fiber and the lack of an active polarization compensation system in the setup, we were unable to obtain ADEV data beyond 50 s for the 120 km link [50]. Nonetheless, we obtain a below 10 mrad ADEV uncertainty in the deployed fiber for averaging times greater than 10 s. Although we did not specifically monitor the weather conditions for the duration of the measurement, this Allan variance measurement shows that the conditions were stable on the scale of ≈ 10 s.

We expect that better interferometric visibility and phase stability can be achieved in the same or similar arrangement by further optimizing the stabilization algorithm and photon count rates and switching to buried fiber as opposed to aerial deployed fiber. Particularly, the RF generation latency of the feedback electronics can be reduced and AOMs can be replaced with electro-optic modulators. These may allow for faster feedback that is equivalent to the higher phase stabilization bandwidth. In addition, the use of better single-photon detectors, e.g., with lower latency and recovery time, could significantly improve the optimization space of future implementations.

4. SUMMARY

We have demonstrated that displacement measurement can be used for Fisher information-enhanced phase tracking and stabilization with single-photon counting in long fiber links. We show experimentally that our method yields Fisher information above that of classical homodyne or heterodyne detection. We have implemented the phase stabilization algorithm with a duty factor of 50% to allow time-division multiplexing of user faint probe signals and quantum payloads. We use attenuated laser light with an average of just $\approx 650,000$ photons per second as a probe signal, which is more than 4 orders of magnitude lower than the probe signal optical power of conventional phase stabilization techniques. We measure the integrated phase noise from 1 Hz to the highest measured frequency of 110 mrad corresponding to rms timing jitter below 0.09 fs in fiber spools and 140 mrad corresponding to rms timing jitter of ≈ 0.12 fs in 120 km deployed fiber.

Our experiments demonstrate high interference visibility and a substantial reduction in phase noise, highlighting the effectiveness of our method. We confirm the long-term phase stability of phase-locked SMF fiber links by calculating the Allan deviation. Beyond sharing phase reference between two parties, this protocol enables the coexistent multiplexing of quantum and faint classical traffic in the same fiber. Our work enables the demonstration of quantum phenomena, such as metropolitan-scale single-photon non-locality, and represents a significant step toward scalable and robust quantum networks, paving the way for future advancements in quantum communication technologies.

Disclosures. The authors declare no conflicts of interest.

Declaration. Certain commercial entities, equipment, or materials may be identified in this document in order to describe an experimental procedure or concept adequately. Such identification is not intended to imply recommendation or endorsement by the National Institute of Standards and Technology, nor is it intended to imply that the entities, materials, or equipment are necessarily the best available for the purpose.

Data availability. Data underlying the results presented in this paper are not publicly available at this time but may be obtained from the authors upon reasonable request.

Supplemental document. See Supplement 1 for supporting content.

REFERENCES

1. J. Bienfang, T. Gerrits, P. Kuo, *et al.*, "Single-photon Sources and Detectors Dictionary," *NIST Interagency/Internal Report (NISTIR) - 8486* (2023).
2. H. J. Kimble, "The quantum internet," *Nature* **453**, 1023–1030 (2008).
3. P. Zoller, T. Beth, D. Binosi, *et al.*, "Quantum information processing and communication," *Eur. Phys. J. D* **36**, 203–228 (2005).
4. S. Wehner, D. Elkouss, and R. Hanson, "Quantum internet: a vision for the road ahead," *Science* **362**, eaam9288 (2018).
5. P. Kómár, E. M. Kessler, M. Bishof, *et al.*, "A quantum network of clocks," *Nat. Phys.* **10**, 582–587 (2014).
6. N. Gisin, G. Ribordy, W. Tittel, *et al.*, "Quantum cryptography," *Rev. Mod. Phys.* **74**, 145–195 (2002).
7. J.-W. Pan, D. Bouwmeester, H. Weinfurter, *et al.*, "Experimental entanglement swapping: entangling photons that never interacted," *Phys. Rev. Lett.* **80**, 3891–3894 (1998).
8. S. Muralidharan, L. Li, J. Kim, *et al.*, "Optimal architectures for long distance quantum communication," *Sci. Rep.* **6**, 20463 (2016).
9. W. J. Munro, K. Azuma, K. Tamaki, *et al.*, "Inside quantum repeaters," *IEEE J. Sel. Top. Quantum Electron.* **21**, 78–90 (2015).
10. M. Żukowski, A. Zeilinger, M. A. Horne, *et al.*, "'Event-ready-detectors' Bell experiment via entanglement swapping," *Phys. Rev. Lett.* **71**, 4287–4290 (1993).
11. E. T. Khabiboulline, J. Borregaard, K. De Greve, *et al.*, "Optical interferometry with quantum networks," *Phys. Rev. Lett.* **123**, 070504 (2019).
12. I. Burenkov, M. Jabir, A. Battou, *et al.*, "Time-resolving quantum measurement enables energy-efficient, large-alphabet communication," *PRX Quantum* **1**, 010308 (2020).
13. M. V. Jabir, N. F. R. Annafianto, I. A. Burenkov, *et al.*, "Versatile quantum-enabled telecom receiver," *AVS Quantum Sci.* **5**, 015001 (2023).
14. I. A. Burenkov, M. V. Jabir, and S. V. Polyakov, "Practical quantum-enhanced receivers for classical communication," *AVS Quantum Sci.* **3**, 025301 (2021).
15. L. Yang, R. Dang, C. Song, *et al.*, "Reference phase stabilizer for distributed underwater sonar systems," *Sensors* **18**, 4279 (2018).
16. Y. Lu, T. Zhu, L. Chen, *et al.*, "Distributed vibration sensor based on coherent detection of phase-OTDR," *J. Lightwave Technol.* **28**, 3243–3249 (2010).
17. L. Hu, X. Tian, L. Wang, *et al.*, "Passive optical phase stabilization on a ring fiber network," *J. Lightwave Technol.* **38**, 5916–5924 (2020).
18. L.-S. Ma, P. Jungner, J. Ye, *et al.*, "Delivering the same optical frequency at two places: accurate cancellation of phase noise introduced by an optical fiber or other time-varying path," *Opt. Lett.* **19**, 1777–1779 (1994).

19. C. E. Calosso, E. K. Bertacco, D. Calonico, *et al.*, “Doppler-stabilized fiber link with 6 dB noise improvement below the classical limit,” *Opt. Lett.* **40**, 131–134 (2015).
20. P. A. Williams, W. C. Swann, and N. R. Newbury, “High-stability transfer of an optical frequency over long fiber-optic links,” *J. Opt. Soc. Am.* **25**, 1284–1293 (2008).
21. N. Deng, Z. Liu, X. Wang, *et al.*, “Distribution of a phase-stabilized 100.02 GHz millimeter-wave signal over a 160 km optical fiber with 100.02 GHz instability,” *Opt. Express* **26**, 339–346 (2018).
22. A. Zhang, Y. Dai, F. Yin, *et al.*, “Phase stabilized downlink transmission for wideband radio frequency signal via optical fiber link,” *Opt. Express* **22**, 21560–21566 (2014).
23. H. Jiang, F. Kéfélian, S. Crane, *et al.*, “Long-distance frequency transfer over an urban fiber link using optical phase stabilization,” *J. Opt. Soc. Am.* **25**, 2029–2035 (2008).
24. I. A. Burenkov, A. Semionov, Hala, *et al.*, “Synchronization and coexistence in quantum networks,” *Opt. Express* **31**, 11431–11446 (2023).
25. J. M. Thomas, G. S. Kanter, and P. Kumar, “Designing noise-robust quantum networks coexisting in the classical fiber infrastructure,” *Opt. Express* **31**, 43035–43047 (2023).
26. L.-J. Wang, K.-H. Zou, W. Sun, *et al.*, “Long-distance copropagation of quantum key distribution and terabit classical optical data channels,” *Phys. Rev.* **95**, 012301 (2017).
27. C. Clivati, A. Meda, S. Donadello, *et al.*, “Coherent phase transfer for real-world twin-field quantum key distribution,” *Nat. Commun.* **13**, 157 (2022).
28. H. Goto, Y. Yanagihara, H. Wang, *et al.*, “Observation of an oscillatory correlation function of multimode two-photon pairs,” *Phys. Rev.* **68**, 015803 (2003).
29. K. Wakui, H. Takahashi, A. Furusawa, *et al.*, “Photon subtracted squeezed states generated with periodically poled KTiOPO₄,” *Opt. Express* **15**, 3568–3574 (2007).
30. Z. Y. Ou and Y. J. Lu, “Cavity enhanced spontaneous parametric down-conversion for the prolongation of correlation time between conjugate photons,” *Phys. Rev. Lett.* **83**, 2556–2559 (1999).
31. S. Izumi, M. Takeoka, K. Wakui, *et al.*, “Optical phase estimation via the coherent state and displaced-photon counting,” *Phys. Rev.* **94**, 033842 (2016).
32. M. Protte, T. Schapeler, J. Sperling, *et al.*, “Low-noise balanced homodyne detection with superconducting nanowire single-photon detectors,” *Opt. Quantum* **2**, 1–6 (2024).
33. B. Hacker, K. Günthner, C. Rößler, *et al.*, “Phase-locking an interferometer with single-photon detections,” *New J. Phys.* **25**, 113007 (2023).
34. S. Yanikgonul, R. Guo, A. Xomalis, *et al.*, “Phase stabilization of a coherent fiber network by single-photon counting,” *Opt. Lett.* **45**, 2740–2743 (2020).
35. D. Pulford, C. Robillard, and E. Huntington, “Single photon locking of an all-fiber interferometer,” *Rev. Sci. Instrum.* **76**, 063114 (2005).
36. V. Makarov, A. Brylevski, and D. R. Hjelm, “Real-time phase tracking in single-photon interferometers,” *Appl. Opt.* **43**, 4385–4392 (2004).
37. N. R. Newbury, P. A. Williams, and W. C. Swann, “Coherent transfer of an optical carrier over 251 km,” *Opt. Lett.* **32**, 3056–3058 (2007).
38. C. W. Chou, H. de Riedmatten, D. Felinto, *et al.*, “Measurement-induced entanglement for excitation stored in remote atomic ensembles,” *Nature* **438**, 828–832 (2005).
39. S. M. Tan, D. F. Walls, and M. J. Collett, “Nonlocality of a single photon,” *Phys. Rev. Lett.* **66**, 252–255 (1991).
40. L.-M. Duan, M. D. Lukin, J. I. Cirac, *et al.*, “Long-distance quantum communication with atomic ensembles and linear optics,” *Nature* **414**, 413–418 (2001).
41. S. L. Braunstein and C. M. Caves, “Statistical distance and the geometry of quantum states,” *Phys. Rev. Lett.* **72**, 3439–3443 (1994).
42. M. T. Jaekel and S. Reynaud, “Quantum limits in interferometric measurements,” *Europhys. Lett.* **13**, 301 (1990).
43. C. W. Helstrom, “Quantum detection and estimation theory,” *J. Stat. Phys.* **1**, 231–252 (1969).
44. R. S. Bondurant, “Near-quantum optimum receivers for the phase-quadrature coherent-state channel,” *Opt. Lett.* **18**, 1896–1898 (1993).
45. S. Guha, J. L. Habif, and M. Takeoka, “Approaching Helstrom limits to optical pulse-position demodulation using single photon detection and optical feedback,” *J. Mod. Opt.* **58**, 257–265 (2011).
46. A. Litvinenko, A. Kumar, M. Rajabali, *et al.*, “Phase noise analysis of mutually synchronized spin Hall nano-oscillators,” *Appl. Phys. Lett.* **122**, 222401 (2023).
47. S. M. Foreman, A. D. Ludlow, M. H. G. de Miranda, *et al.*, “10⁻¹⁷ Coherent optical phase transfer over a 32-km fiber with 1 s instability at,” *Phys. Rev. Lett.* **99**, 153601 (2007).
48. W. J. Riley, W. J. Riley, and J. A. Barnes, *Handbook of Frequency Stability Analysis* (NIST, 2008).
49. J. Hamilton, “Stable32: frequency stability analysis software,” <http://www.wiley.com> (2005).
50. W. McKenzie, A. M. Richards, S. Patel, *et al.*, “Clock synchronization characterization of the Washington DC metropolitan quantum network (DC-QNet),” *Appl. Phys. Lett.* **125**, 164004 (2024).